Pharm Res (2014) 31:2439–2452
DOI 10.1007/s11095-014-1339-x

RESEARCH PAPER

Uptake and Cytotoxicity of Docetaxel-Loaded Hyaluronic Acid-Grafted Oily Core Nanocapsules in MDA-MB 231 Cancer Cells

Ibrahima Youm • Vivek Agrahari • James B. Murowchick • Bi-Botti C. Youan

Received: 18 September 2013 / Accepted: 13 February 2014 / Published online: 19 March 2014

ABSTRACT

Purpose It is hypothesized that docetaxel (Doc)-loaded hyaluronic acid (HA)-polyethylene glycol/poly(ε-caprolactone)-grafted oily core nanocapsules (NCs) can enhance the drug cytotoxicity and uptake in CD44 expressing breast cancer (BC) cells (MDA-MB 231).

Methods NCs were prepared, optimized and characterized by dynamic light scattering, transmission electron microscopy (TEM), and powder X-ray diffraction (PXRD). *In vitro* cytotoxicity tests [MTS, level of reactive oxygen species (ROS) and level of reduced glutathione (GSH)] were performed in BC cells. The contribution of CD44 to the NCs cellular uptake was elucidated using an anti CD44 antibody blockage *and a CD44 negative NIH3T3 cell line*.

Results The optimum formulation of Doc-loaded HA oily core NCs had respective mean diameter, polydispersity, and drug encapsulation efficiency of *224.18 nm, 0.32*, and *60.38%*. The NCs appeared spherical with low drug crystallinity, while the drug release data fitted to first order equation. Compared to that of ungrafted NCs, the cytotoxicity of Doc-loaded HA-grafted NCs was significantly enhanced ($p<0.05$). A decrease of the intracellular level of ROS was reversely correlated with that of GSH. Interestingly, the cellular internalization of HA-grafted NCs mediated CD44 was *dramatically* enhanced *(3 to 4-fold) with respect to the absence of specific biomarker or targeting ligand.*

Conclusions The use of HA-grafted NCs enhanced the *selective* drug payload, cytotoxicity and uptake in *MDA-MB 231 cells. Therefore, it could be a* promising template for safe and effective delivery *of* Doc and similar *chemotherapeutic agents in cancer cells.*

KEY WORDS breast cancer · cancer chemotherapy · CD44 receptor · cytotoxicity · hyaluronic acid · nanocapsules · particle cellular uptake

Electronic supplementary material The online version of this article (doi:10.1007/s11095-014-1339-x) contains supplementary material, which is available to authorized users.

I. Youm · V. Agrahari · B.-B. C. Youan (✉)
Laboratory of Future Nanomedicines and Theoretical Chronopharmaceutics, Division of Pharmaceutical Sciences
University of Missouri-Kansas City, 2464 Charlotte Street
Kansas City, Missouri 64108, USA
e-mail: youanb@umkc.edu

J. B. Murowchick
Department of Geosciences
University of Missouri-Kansas City, 420 Flarsheim Hall, 5110 Rockhill Rd.
Kansas City, Missouri 64110, USA

INTRODUCTION

The two major challenges in the field of drug delivery include selective drug targeting to diseased tissues and reduced side effects. In the case of breast cancer (BC), the lack of specific biomarkers is one of the major limitations for effective diagnosis and therapy. Therefore, the formulation of a nanocarrier bearing efficient and active target molecules becomes challenging for the development of novel BC therapies. Hence, different strategies have been proposed as possible approaches for active targeting in BC. These included peptides, biodegradable polymers, antibodies, aptamers, siRNA, and aptamer-siRNA chimera (1–4). Hyaluronic acid (HA) *is a glycosaminoglycan that* has been proposed as a new candidate for active targeting of CD44 *(cluster of differentiation 44)*, intended for the treatment of melanoma (5).

HA is a water soluble, biodegradable, biocompatible, non-toxic, non-immunogenic, and an important constituent of the extracellular matrix (5,6). More interestingly, HA is endowed with a strong receptor binding capability to CD44 and hyaluronan-mediated motility receptor that confers its target ability to CD44 expressing BC cells (7). Ligand binding of CD44 has been associated with many cellular processes such as migration, adhesion, signaling, and proliferation (8). CD44 is the principal cellular surface receptor for HA that has been found in many cells and tissues including breast tumor cells and carcinoma tissues (9). The mechanism by which cancer cells acquire the ability to evade and migrate from the primary

to the secondary sites is a critical process in the development of metastatic cancer. In BC, the influence of HA on cell migration has been clinically shown to be CD44 dependent (10). In addition, pathological conditions have been correlated with the enhancement of the HA binding to CD44 that lead to increased tumor progression (7,11). Therefore, the use of HA/CD44 *interactions* to actively target *advanced breast carcinoma* could be a promising approach.

In this study, docetaxel (Doc), a lipophilic anticancer agent was selected as a model drug. Parenteral formulation of Doc containing 4% Tween® 80 w/v is approved for breast and ovary cancer chemotherapy (12). However, this latter formulation encounters some limitations due to the presence of Tween® 80, which causes hemolysis and other allergies in patients (13). To overcome these drawbacks, we synthesized surfactant-free nanocapsules (NCs) based biocompatible polymers with high drug payload. Hence, HA-conjugated polyethylene glycol/poly(ε-caprolactone, PEG/PCL) was used to synthesize Doc-loaded HA-PEG/PCL-grafted NCs. The hydrophilic nature of PEG combined with HA could represent the hydrophilic moiety of the conjugate. Ligand (HA) attachment to PEG on the surface of such small-sized NCs (<200 nm) could concomitantly allow prolonging the NCs systemic circulation time, *and enhance* the permeability and retention (EPR) effect (14). In addition to the PCL moiety, the hydrophobic oily core of the synthesized NCs could allow a high encapsulation efficiency of hydrophobic drugs through hydrophobic interactions.

We hypothesize that Doc-loaded HA-PEG/PCL-grafted NCs can enhance *in vitro* the NCs uptake and cytotoxic activity of Doc against the CD44 expressing BC cells, namely MDA-MB 231. The newly synthesized NCs were optimized using Box-Behnken experimental design (BBD) *including six center-points* (15). BBD was used to minimize the number of runs during the process of optimization. Furthermore, the physicochemical characteristics and the effect of the freeze-drying on the NCs mean diameter were also analyzed.

In vitro cytotoxicity of the synthesized NCs was investigated to test the potential toxicity of Doc-loaded HA-PEG/PCL-grafted NCs in cancer cells. For the particle cellular uptake study, the NCs were fluorescently labeled to quantify and monitor their internalization in MDA-MB 231 cells. Furthermore, the involvement of the CD44 receptors in the particle cellular internalization was tested *using an anti-CD44 antibody and a CD44-negative NIH3T3 cell line.*

MATERIALS AND METHODS

Materials

Docetaxel (Doc) was supplied by LC Laboratories (Woburn, MA). Amine polyethylene glycol/Poly(ε-caprolactone, PEG/PCL, 5–10kDa) diblock was purchased from Advanced Polymers Material Inc (Montréal, Canada). Hyaluronic acid (Mw: 11.6 kDa) was kindly provided by Zhenjiang Dong Yuan Biotech Co., Ltd. (Jiangsu, China). APC anti-mouse/human CD44 antibody was supplied by BioLegend Inc. (San Diego, CA). Labrafac®CC oil (caprylic/capric triglyceride, d=0.945 g/cm^3) was a kind gift from Gattefosse Corporation (St-Priest, France). Potassium phosphate monobasic (KH_2PO_4), phosphate buffered saline (PBS), *deuterated water (D_2O), dim*ethylsulfoxide (DMSO), *deuterated DMSO (d_6-DMSO),* ethanol, methanol, N-hydroxysuccinimide (NHS), *hydrogene peroxide (H_2O_2), Triton™ X-100,* and propidium iodide (PI) were purchased from Sigma Aldrich (St. Louis, MO). 1-Ethyl-3-(3-dimethylaminopropyl) carbodiimide hydrochloride (EDC) was provided by Thermo Fisher Scientific (Rockford, IL). Dichloromethane (DCM) was supplied by Acros Organics (Morris Plains, NJ). Acetonitrile, ethanol and formic acid were provided by Fisher Scientific (Pittsburgh, PA). Monochlorobimane (MCB), camptothecin (CPT) and 2′,7′-dichlorofluorescin diacetate (H2DCFDA) were purchased from Sigma Aldrich (St-Louis, MO). Sodium hydroxide (NaOH) was obtained from Fisher Scientific Company LLC (Hanover Park, IL). Fluorescein isothiocyanate (FITC) was obtained from Invitrogen Corporation (Carlsbad, CA). CytoTox-ONE™ and CellTiter 96™ aqueous kits were provided by Promega (Madison, WI). All solvents were of analytical grade and used without further purification.

Synthesis of Hyaluronic Acid-Conjugated Polyethylene Glycol/Poly(ε-caprolactone)

The conjugation of amine PEG/PCL with HA was performed using carbodiimide coupling reaction (Fig. 1) (16). The carboxylic acid group of HA were activated with EDC and stabilized with NHS. An amount of HA (0.23 μmol) was mixed with EDC (7.82 μmol) and NHS (39.10 μmol), and then dissolved in 1 mL of phosphate buffer (0.1 M, pH 6.2). The solution was stirred to modify the carboxyl ligands of HA with NHS. *After 30 min*, the excess of EDC and NHS was removed by dialysis (Spectra/por Float-A-Lyzer G2, MWCO 3.5–5 kDa Spectrum Laboratories Inc. Rancho Dominguez, CA) *against deionized water at room temperature for 3 h.* Then, the amine PEG/PCL solution (4 mg in 1 mL of DMSO) was added to the activated HA solution and stirred for 24 h at room temperature. The obtained solution was suspended in 95% ethanol to precipitate the free HA and centrifugated *(VWR International Micro 18R, Darmstadt, Germany)* at 15,000 rpm for 30 min at 8°C. The supernatant containing HA-PEG/PCL conjugate was recovered in purified water (Direct-Q 3 UV system, Millipore SAS, Molsheim, France), freeze dried, and stored at 8°C until further use.

Proton nuclear magnetic resonance spectroscopy

Proton nuclear magnetic resonance (^{1}H NMR) spectroscopy was performed to characterize the synthesized HA-PEG/PCL

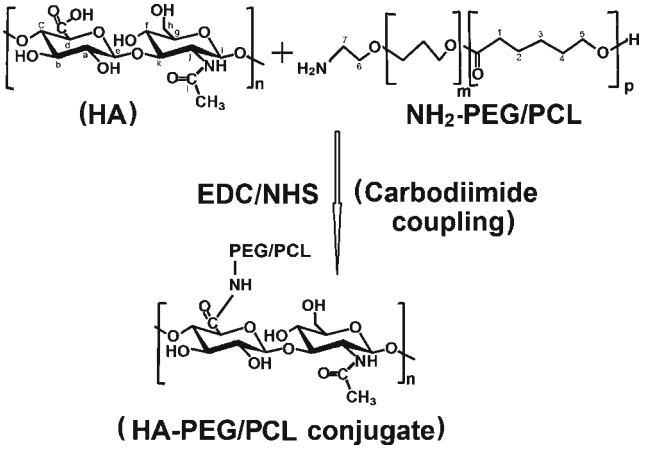

Fig. 1 Schematic diagram of the synthesis of hyaluronic acid-polyethylene glycol/poly(ε-caprolactone) conjugate using carbodiimide chemistry.

conjugate. Samples of NH_2-PEG/PCL and HA-PEG/PCL copolymers were dissolved in d_6-DMSO and transferred into NMR glass tubes. In turn, the HA sample was dissolved in D_2O since d_6-DMSO is not a good solvent to record the NMR spectra of unmodified hydrophilic HA. The spectra were acquired at room temperature using a Varian Inova 400 MHz spectrometer (Varian, Palo Alto, CA). The ^{1}H-NMR spectra were recorded between 14 to −2 ppm using a relaxation delay time of 1 s. Chemical shift values are reported in parts per million (ppm).

Optimization of the Formulation of Docetaxel-Loaded Hyaluronic Acid-Polyethylene Glycol/Poly(ε-caprolactone)-grafted Oily Core Nanocapsules

Doc-loaded HA-PEG/PCL-grafted oily core NCs were prepared using an oil-in-water emulsion solvent diffusion method (17). Briefly, known amounts of HA-PEG/PCL were dissolved in 8 mL of water-saturated ethyl acetate (internal phase). Then, the Labrafac®CC oil (0.2 to 0.6 ml) containing Doc (2 to 6 mg) was added to the internal phase (Supplementary Material Table S1). The latter solution was added dropwise in 40 mL ethyl acetate saturated water (external phase) and homogenized for 10 min at 8,300 rpm (IKA ULTRA-TURRAX T-25, Staufen, Germany). To promote the diffusion of the internal phase toward the external phase, the emulsion was added dropwise into 100 mL of deionized water (*Direct-Q 3 UV system, Millipore SAS, Molsheim, France*) and maintained under constant stirring for 2 h at room temperature. The residual ethyl acetate was evaporated at 40°C for 30 min under reduced pressure (Rotavapor® RII, BUCHI Labor technik AG, Flawil, Switzerland). The unreacted formulation components were removed by dialysis using deionized water every three hours for 12 hours. Doc-loaded HA-PEG/PCL-grafted NCs were collected by *ultracentrifugation (L8-70 M ultracentrifuge, Beckman Coulter Inc. Brea, CA)* at 20,000 rpm for 30 min at 5°C. The NCs were suspended in an aqueous phase containing 2% (w/v) trehalose (*used as a cryoprotectant*) and then freeze dried (Freezone Lab Scale System, Labconco Corp. Kansas City, MO). Fluorescein isothiocyate (FITC)-loaded HA-grafted or ungrafted NCs (*Blank NCs*) were also prepared using the above method.

Experimental Design

For the optimization of the NCs, a three-factor, three-coded level Box Behnken design (BBD) *with six center-points* was constructed (Supplementary Material Table S1). The statistical analysis of the factorial design formulation was performed using JMP software version 8.02 (SAS Institute, Cary, NC) as previously reported (18).

Characterization of Docetaxel-Loaded Hyaluronic Acid-Polyethylene Glycol/Poly(ε-caprolactone)-grafted Oily Core Nanocapsules

Particle Mean Diameter and Polydispersity Analysis

The analysis of the NCs mean diameter (PMD) and polydispersity index (PDI) was performed using dynamic light scattering (DLS) method (Zetasizer Nano ZS, Malvern Instruments Ltd, Worcestershire, UK) at 25°C. Two milligrams of freeze-dried NCs were dispersed in 1 mL of deionized water. Then 100 μL of the colloidal suspension was withdrawn, diluted 10 times in purified water to dissolve the residual cryoprotectant. Before analysis, the particle suspension was sonicated for 2 min under ice (Misonix Sonicator 300, Misonix Inc., Farmingdale, NY). According to the National Institute of Standards and Technology (NIST), a sample with a PDI < 0.05 is considered monodisperse (19).

Determination of the Encapsulation Efficiency of Docetaxel-Loaded Hyaluronic Acid-Polyethylene Glycol/Poly(ε-caprolactone)-grafted Oily Core Nanocapsules

The powdered NCs (2-3 mg) were dissolved in 0.1 mL of DCM and diluted in methanol at the ratio of 1:14 v/v (18). The obtained mixture was centrifugated at 15,000 rpm for 20 min at 8°C. The amount of Doc was determined from the supernatant using a high performance liquid chromatography (HPLC) method (20). Theoretical drug loading (DL%) and *percent drug encapsulation efficiency* (EE%) were calculated according to Eqs. 1 and 2:

$$DL\ \% = \frac{Drug\ \ amount}{Amount\ \ of\ \ polymer + Drug\ \ amount} \times 100 \qquad (1)$$

$$EE\,\% = \frac{Experimental\ \ drug\ \ loading}{Theoretical\ \ drug\ \ loading} \times 100 \quad (2)$$

Morphological Analysis of Docetaxel-Loaded Hyaluronic Acid-Polyethylene Glycol/Poly (ε-caprolactone)-grafted Oily Core Nanocapsules

The morphology of NCs was analyzed using a transmission electron microscope (TEM). The NCs were diluted in a 2.5% aqueous solution of uranyl acetate (UA) *and* sonicated. A volume of 8 μL of the colloidal dispersion was put on a carbon-coated grid for equilibration. After 5 min, a 5% aqueous solution of UA was poured on the grid to increase the contrast. The grids were viewed under a TEM (Philips CM12 STEM, San Jose, CA) equipped with the large format (II Megapixel), retractable, and fiber-optical coupled SC100 ORIUS© CCD camera for digital image acquisition.

Powder X-Ray Diffraction (PXRD) Pattern Analysis

The PXRD analysis of powdered NCs was performed using a Rigaku MiniFlex automated X-ray diffractometer (Rigaku, The Woodland, TX) at room temperature. An Ni-filtered Cu Kα radiation was used at 30 kV and 15 mA. The diffraction angle varied from $2\theta=5°$ to $2\theta=50°$ with a step size of 0.05°/step, and a count time of 2.5 s/steps (1.2°/min). The diffraction patterns were processed using Jade 8+ software (Materials Data, Inc., Livermore, CA).

Effect of the Freeze Drying Process on the Particle Mean Diameter

Three milligrams of powdered NCs of each formula were suspended in 5 mL of phosphate buffered saline (PBS) at 37°C. The samples were diluted 5 times with PBS, sonicated for 2 min and analyzed by DLS. The PMD of the freeze dried NCs was determined and compared to that of freshly prepared NCs using the final to initial size ratio (S_F/S_I).

In Vitro Drug Release Analysis

In vitro drug release *of native Doc or* from Doc-loaded HA-PEG/PCL-grafted NCs was performed using a dialysis method. Specifically, a known amount of *native Doc or* powdered Doc-loaded HA-grafted NCs corresponding to 2 mg of Doc was suspended in a dialysis bag (spectra/Por Float-A-Lyzer G2, MWCO 2.5–5 kDa, Spectrum Laboratories Inc, Rancho Dominguez, CA) containing 5 mL of PBS solution (0.1 M at pH 7.4 *and 0.1% v/v of Tween 80*). The bag containing the NCs suspension was placed *in a 50-mL Eppendorf® tube (Fisher Scientific Company LLC, Houston, TX)* containing 40 mL of PBS solution *and 0.1% v/v of Tween 80*. The whole system was then placed in a shaking water bath (BS-06, Lab. Companion, Des Plaines, IL) at 37°C *at* agitation speed of 50 rpm *for 12 h*. At various time points, the samples were collected and the release medium was replaced with 200 μL of fresh medium to maintain the sink conditions. The percent drug release was calculated as percentage of the total encapsulated drug. *Furthermore*, the *in vitro* drug release data were fitted to various kinetic models to elucidate the drug release mechanism and kinetics (21).

Cell Culture Condition

Human breast carcinoma cells (MDA-MB 231) from American Type Culture Collection (ATCC, Manassas, VA) were grown in Dulbecco's Modified Eagle's Medium (DMEM) high glucose supplemented with 1% v/v Minimum Essential Medium Non-Essential Amino Acid solution, 2 mM glutamine (Sigma Aldrich, Saint-Louis, MO), 10% v/v fetal bovine serum (FBS, ATCC), 1% v/v penicillin-streptomycin (Gibco BRL, Grand Island, NY), and 1.7% v/v MEM-Vitamin (Thermo Scientific, Rockford, IL). *NIH3T3 cells from ATCC were grown in DMEM high glucose containing 10% v/v of FBS. Both* cells were maintained in growth phase by completing the passage every three days in a T-25 flask (MIDSCI, Saint-Louis, MO) containing *3 mL of complete* growth medium in a humidified incubator at 37°C in 5% CO_2.

Cell Viability Assay

A cell viability assay was performed using methyl tetrazolium salt (MTS) assay following the manufacturer's instruction. MDA-MB 231 cells (5×10^5/well) were transferred into 96-well plates until 80% confluence. The growth medium was replaced with 100 μL of fresh medium or 1% v/v Triton X-100 as negative and positive controls, respectively. Known amounts of native Doc, Doc-loaded PEG and Doc-loaded HA-PEG/PCL-grafted NCs corresponding to 10,000 nM of Doc were suspended in a complete culture medium and sonicated for 2 min. Furthermore, the samples were serially diluted in the complete growth medium from 10,000 nM to 0.01 nM. For treatments, cells were incubated with 100 μL of medium containing blank NCs, native Doc, or an equivalent amount of Doc containing PEG NCs and HA-PEG/PCL-grafted NCs at different concentrations at 37°C in 5% CO_2. After 24 h, the cells were incubated with an additional 20 μL of CellTiter 96® Aqueous One Solution Reagent (Promega, Madison, WI) for 4 h. After the completion of the exposure period, the 96-well plate was placed on a DTX 800 multimode microplate reader (Beckman Coulter, Brea, CA) and the absorbance of the formazan product was measured at 490 nm. The cell viability was determined using the below equation:

$$Cell\ viability\ (\%) = \frac{Absorbance\ of\ treated\ cells}{Absorbance\ of\ untreated\ cells} \times 100 \quad (3)$$

Detection of Intracellular Reactive Oxygen Species Accumulation

The intracellular concentration of reactive oxygen species (ROS) was estimated using the intracellular level of H_2DCFDA that forms a green fluorescent when associated with ROS (22). The H_2DCFDA measures the peroxides (*e.g.*, hydrogen peroxide: H_2O_2 and lipid peroxide) that can be used to further generate other ROS. After 20 min of incubation with 7 μM of H_2DCFDA, the cells were rinsed twice with PBS. Fluorescence was monitored by scanning the 96-well plate using excitation and emission wavelengths of 485 and 535 nm, respectively. For each well, the fluorescence value was corrected with the intracellular content of proteins. The values were expressed as number of folds compared to "control" wells. Samples treated with 3% of H_2O_2 were used as a positive control.

Measurement of Intracellular Reduced Glutathione

Three independent experiments were carried out using native Doc, Doc-loaded PEG, and Doc-loaded HA-PEG/PCL-grafted NCs. The content of intracellular reduced glutathione (GSH) was determined using monochlorobimane (MCB, 40 μM) (23). MCB was utilized as a probe that reacts with GSH generating a detectable MCB-GSH conjugate by fluorimetry. After 20 min of incubation in culture media containing MCB, the cells were washed twice with cold HEPES buffer. Fluorescence was detected by scanning the 96-well plates using an excitation wavelength of 360 nm and an emission wavelength of 465 nm. For each well, the fluorescence of MCB was calculated as previously described (23). The final fluorescence values were corrected for intracellular protein in each well and expressed as a percent of fluorescence. Camptothecin (CPT, 20 μM), a topoisomerase inhibitor, was used as positive control.

Particle Cellular Uptake Study by Microplate Reader

MDA-MB 231 *and NIH3T3 (mouse embryonic fibroblast)* cells were *separately* cultured in a T-25 flask until 80% confluence, then transferred to 96-well plate to ensure 2.5×10^4 cells per well. Cells were incubated in 100 μL of *complete growth* medium containing FITC-loaded HA-PEG/PCL-grafted NCs or FITC-loaded PEG NCs at different concentrations (37.5, 75, and 150 μg/mL) for 24 h. The *complete growth* medium containing cells with blank NCs was used as *background*. After incubation, the suspension was removed and the *cells* were washed three times using PBS solution.

Particle Cellular Uptake Study by Flow Cytometry Analysis

The quantification of the percent of FITC-loaded NCs cellular uptake was also investigated using flow cytometry. MDA-MB 231 cells (2.5×10^5 cells/mL) were seeded in two sets of four T-25 flasks (including tested samples and control : unlabeled NCs) under the above condition for 24 h. Cells were incubated in 2.5 mL of culture medium containing FITC-loaded HA-PEG/PCL-grafted or PEG NCs at different concentrations of FITC (37.5, 75, and 150 μg/mL). After 24 h, cells were washed three times with PBS and harvested using 2 mL of 0.25% trypsin-EDTA solution (Sigma Aldrich, Saint-Louis, MO) for 6 min, then diluted with an equal volume of FBS. Cells were collected by centrifugation (3000 rpm for 10 min) and resuspended in 5 mL test tubes (BD Biosciences, San Jose, CA) containing 2 mL of fresh complete culture medium. The number of cells containing FITC-loaded NCs, as well as their fluorescence intensity, was measured using the BD LSR II Flow Cytometer (BD Biosciences).

Particle Cellular Uptake Study by Confocal Microscopy

MDA-MB 231 cells were incubated in 16-well glass slides. After 80% confluence, the *growth* medium was replaced with 100 μL of FITC-loaded HA-PEG/PCL-grafted or FITC-loaded PEG NCs (37.5, 75, and 150 μg/mL). After 24 h of incubation, the cells were washed three times with PBS solution (pH 7.4). *A volume of 20 μL* of 70% ethanol solution was added to each well for cell fixation at 37°C for 20 min. After step-washing three times with PBS solution, a volume 10 μL of PI (5 mg/mL) was subsequently added to each well to stain the cell nucleus. After 40 min, cells were washed three times with PBS solution, the 16-well glass slides was observed by confocal laser scanning microscopy (CLSM, 510 META, Carl Zeiss, Germany) with the following excitation and emission wavelengths for FITC and PI: excitation: 488 nm emission: band pass 505–530 nm; excitation: 536 nm and emission: 617 nm, respectively. The untreated cells were used as a negative control for the microscope settings. The FITC-loaded NCs, PI-staining cell nucleus, and merged images displayed green, red, and yellow color, respectively.

Involvement of CD44 Receptor in the Nanocapsules Internalization

The cellular uptake efficacy of HA-PEG/PCL-grafted NCs *via* HA and CD44 interaction was investigated using two different approaches.

First, MDA-MB 231 and NIH3T3 cells were respectively used as CD44-rich and CD44-negative cell lines. Both cells were incubated in their respective complete medium containing different concentrations of FITC-loaded HA-PEG/PCL

grafted NCs for 24 h at 37°C in 5% CO_2. After incubation, the cells were washed thrice with PBS solution. The percentage of NCs taken up by the cells was calculated according to the ratio between the initial amount of FITC loading (100% in the culture media before incubation) and the final FITC amount found inside the cells at an excitation wavelength of 488 nm and emission wavelength of 525 nm. A calibration curve was constructed by plotting the fluorescence intensity *versus* the corresponding concentrations of FITC (10–400 μg/mL). The coefficient of determination (r^2) of this calibration curve was found to be 0.996.

Second, MDA-MB 231 cells were pretreated with CD44 blocking antibody (2.5 μg/mL) for 3 h and compared to untreated samples. Cells were washed twice with a PBS solution to remove unbound antibodies, and then resuspended in *growth* medium containing 150 μg of FITC-loaded HA-PEG/PCL-grafted and PEG NCs. The subsequent cell treatment procedure was the same as described above. Complete growth medium containing blank NCs stabilized with 1% trehalose was used as control.

Statistical Analysis

Analysis of variance (ANOVA) was used within each treatment and applied among the groups. The results were expressed as means ± standard deviation (SD). A P-value (p) of 0.05 or less was considered statistically significant.

RESULTS AND DISCUSSION

Synthesis of Hyaluronic Acid-Polyethylene Glycol/Poly(ε-caprolactone) Conjugate

In the spectrum of HA, the broad signal between 3.0 and 3.8 ppm corresponds to the signals of the protons in the sugar rings (Fig. 2a). Signals were all super imposed, which makes it difficult to assign each proton individually. However, signals were assigned according to their corresponding protons in the sugar rings. The characteristic signal at around 4.6 ppm corresponds to the two anomeric protons attached to the carbons adjacent to the two oxygen atoms (see label i,e in Fig. 2a). The methyl ($-CH_3$) protons of the N-acetyl group of HA showed a signal at 1.9 ppm. For the NH_2-PEG/PCL copolymer, the characteristic NMR signal at 3.5 ppm was assigned to the ethylene group ($-CH_2CH_2-$) of PEG (see label 6, 7 in Fig. 2b), whereas signals at around 1.3, 1.55, 2.3, and 4 ppm were assigned to the PCL (see label 1, 2, 3, 4 and 5 in Fig. 2b). The proton NMR signals assigned to the spectrum of NH_2-PEG/PCL are given in Fig. 2b. In the spectrum of HA-PEG/PCL conjugate, the formation of the amide (CONH) bond was confirmed by the characteristic proton signal around 5.0 ppm (Fig. 2c). Moreover, Fig. 2c also exhibits the above characteristic peaks of PEG, HA and PCL which further confirm the formation of the new conjugate.

Preparation and Optimization of Docetaxel-Loaded Hyaluronic Acid-Grafted Polyethylene Glycol/Poly (ε-caprolactone) Oily Core Nanocapsules

In our preliminary screening test, Plackett–Burman design was performed to identify the significant variables that could affect the PMD, PDI and EE%. Three independent variables (Doc, HA-PEG/PCL and oil amounts) were found to significantly impact the NCs formulation's targeted product profiles (results not shown). In this study, an experimental design is selected with the goal of obtaining a minimal experimental error, a limited number of runs and a better statistical prediction. In that respect, BBD is the ideal option for 3 factors for fitting quadratic models that requires 3 levels of each factor (24).

The experiments were designed with the ultimate goal of minimizing both the PMD and PDI values while maximizing the EE%. The results from PMD, PDI, and EE% were summarized in Table I. The influence of each factor on the formulation responses was also summarized in Fig. 3. As shown, the PMD was mainly governed by the amount of HA-PEG/PCL and its curvilinear effect ($p<0.001$ and 0.016, respectively, Fig. 3a). However, the main effect of the independent variables and interactions did not exert any significant influence on Y_2 (Fig. 3b). Interestingly, EE% was markedly influenced by the amount of HA-PEG/PCL ($p=0.0251$), and the curvilinear effect of Doc ($p=0.0421$, Fig. 3c). *The optimal formulation of Doc-loaded HA-PEG/PCL-grafted oily core NCs* (F_{opt}) *predicted* by the model had respective PMD, PDI, and EE% of *224.18± 15.71 nm, 0.32± 0.11, and 60.38± 7.70%* (Fig. 4). Furthermore, the comparison between the predicted and the experimental values of the dependent variables was investigated by a check point analysis. As shown in Table II, the differences between the predicted and experimental values appeared to be statistically insignificant ($p>0.05$). This indicated that the model is able to predict the PMD and EE% with high precision in the working design space.

Morphological Analysis

TEM analysis was performed to study the morphology of the optimized formula of Doc-loaded HA-PEG/PCL-grafted NCs. Figure 5a and b *show white, shiny oily cores* and spherical NCs with size measuring 200 nm, which was in good agreement with the results obtained by DLS. The high molecular weight and the concentration of the polymers (HA, PEG, and PCL) used in the formulation of the nanocarriers could lead to increased viscosity of the internal phase during the emulsion, thereby resulting in an increase in the PMD. Similar particle size range was also found by Lui *et al.* (25).

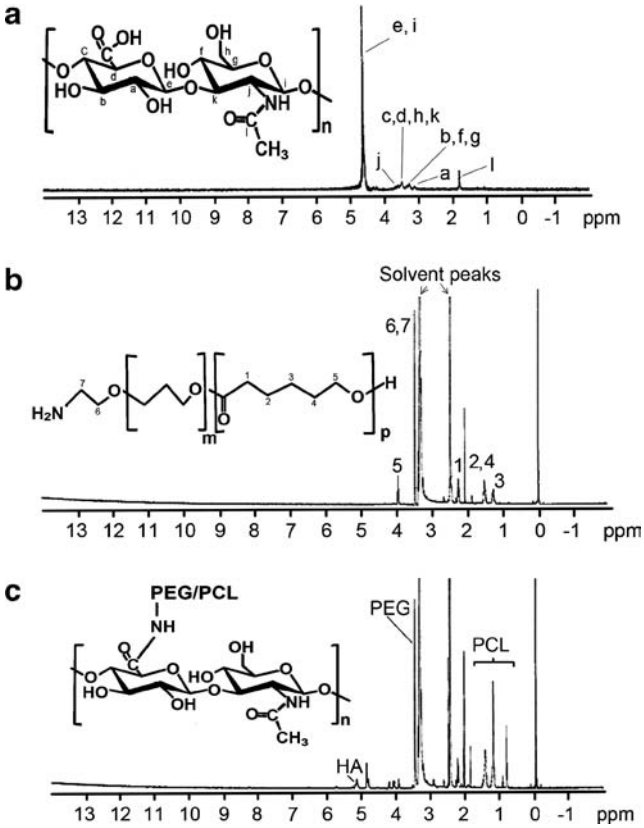

Fig. 2 ^{1}H-NMR spectra of (**a**) hyaluronic acid; (**b**) amine-polyethylene glycol/poly(ε-caprolactone) and (**c**) hyaluronic acid-polyethylene glycol/poly(ε-caprolactone) conjugate.

Powder X-Ray Diffraction Pattern Analysis

In Fig. 5c, the PXRD data showed the presence of crystalline Doc in its characteristic diffraction peaks at 7.3, 8.8, 13.7, 17.2, and 20.2±0.2° two-theta (26). Doc is by nature crystallized in an orthorhombic system with a number of motifs (z) per cell equal to 4. The characteristic unit cell parameters (at room temperature) are a=39.9345 Å, b=12.7749 Å, c=8.6644 Å, with V=4420.2 Å (26). Compared to the physical mixture of Doc + blank NCs, data from Doc-loaded HA-grafted NCs showed characteristic peaks of Doc with reduced intensity. This suggested that the drug encapsulation in the oil phase could lead to a partial amorphization of Doc reducing its crystallinity, which is consistent with previous works (27).

Effect of the Freeze Drying Process on the Particle Mean Diameter

Results indicated that some formulations (F_2, F_3, F_4, F_5, F_6, F_{10} and F_{11}) exhibited a change in PMD without leading to the formation of large aggregates (PMD<500 nm, Fig. S1 in Supplementary Material). The values of the S_F/S_I ratio were between 0.70 and 1.59. The other formulations exhibited similar PMD before and after freeze drying (S_F/S_I near from 1). A complete redispersion of the NCs after freeze drying was difficult to achieve without sonication due to the aggregation (chemically-bound particles) or irreversible agglomeration (physically-bound particles) that can compromise the mobility of the single NCs in the fluid during DLS analysis. Also, freeze-

Table I Box-Benken Experimental Design for Formulation Variables [(Doc (Docetaxel, X_1), HA-PEG/PCL, (X_2) and Oil Volume (X_3)] with Measured Responses [Particle Mean Diameter (PMD, Y_1), Polydidpersity Index (PDI, Y_2) and Drug Encapsulation Efficiency (EE%, Y_3)]

Formulation	Doc amount (mg)	HA-PEG/PCL amount (mg)	Oil volume (mL)	PMD (nm)	PDI	EE%
F_1	4	16	0.6	468.8	0.113	87.1
F_2	4	10	0.4	220.2	0.235	68.2
F_3	6	10	0.2	276.6	0.160	82.0
F_4	4	4	0.2	152.6	0.225	54.7
F_5	2	10	0.6	232.1	0.401	86.2
F_6	2	16	0.4	474.9	0.240	84.8
F_7	4	16	0.2	451.5	0.263	76.3
F_8	4	10	0.4	225.9	0.184	40.9
F_9	2	10	0.2	273.6	0.305	74.3
F_{10}	6	10	0.6	268.9	0.176	70.2
F_{11}	6	16	0.4	522.1	0.421	84.3
F_{12}	4	4	0.6	144.3	0.155	58.3
F_{13}	2	4	0.4	111.6	0.213	70.6
F_{14}	6	4	0.4	165.1	0.114	62.4
F_{15}	4	10	0.4	234.2	0.497	62.7
F_{16}	4	10	0.4	222.6	0.378	64.2
F_{17}	4	10	0.4	224.8	0.316	64.3
F_{18}	4	10	0.4	217.4	0.300	63.8

drying can induce a mechanical stress on particles leading to change in particle size. Similar result has been found in previous work (28).

In Vitro Drug Release Mechanism and Kinetics

At high drug loading, the drug release rate was decreased with high polymer and oil contents (see F_1 *versus* F_2, Fig. 6a). This indicated that the drug release was dictated by the oil and PCL moiety in the lipophilic core of the NCs. This finding was also supported by the following results, where the drug release decreased at low drug content and high polymer content (F_5 and F_9, Fig. 6a and b). To support the hypothesis by which the dialysis membrane is not a rate-limiting barrier for the drug transport into the receiving phase, a native drug release kinetic study was performed in the same condition. The results showed that the release of Doc from the NCs was slower than that of native drug, except for formulation F_{15} (Fig. 6a and c). At a low amount of HA-PEG/PCL, the release of Doc was

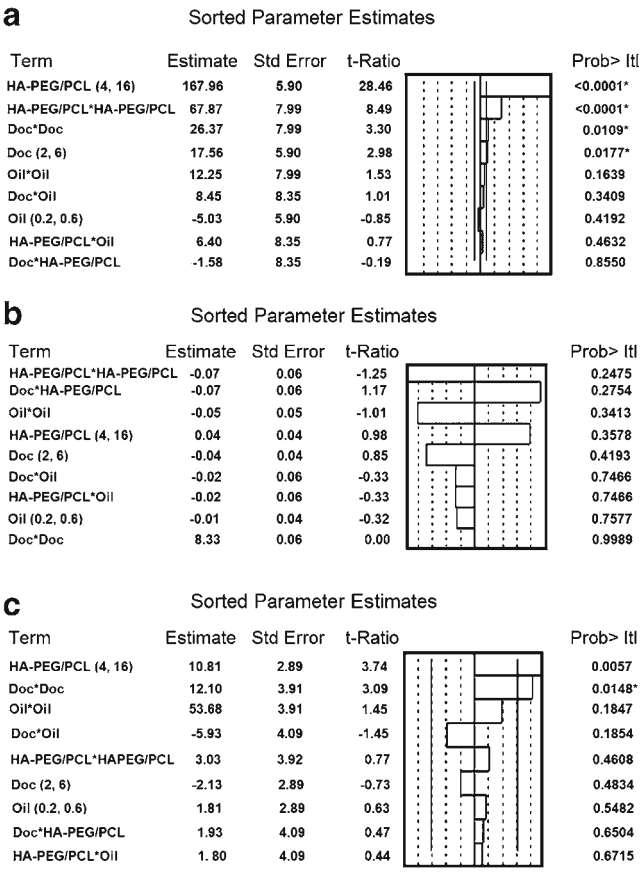

Fig. 3 Pareto chart showing the standardized effect of formulation variables and their interaction on (**a**) particle mean diameter (PMD), (**b**) polydispersity index (PDI) and (**c**) percent drug encapsulation efficiency (EE%) of docetaxel-loaded HA-PEG/PCL-grafted oily core nanoformulations. The two *vertical lines* represented the $t_{critical}$ values. Any *bar* exceeding these *lines* indicated statistical significance ($p<0.05$) for the corresponding effect.

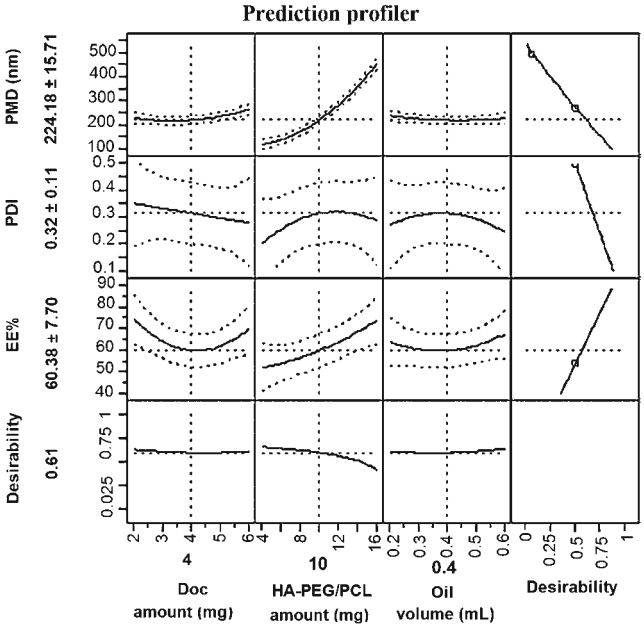

Fig. 4 Prediction and desirability plot showing the effect of docetaxel amount, HA-PEG/PCL amount, and oil volume on the particle mean diameter (PMD), polydispersity index (PDI) and percent drug encapsulation efficiency (EE%) of the HA-PEG/PCL-grafted nanocapsules.

increased (see F_{12}, F_{13} and F_{14}, Fig. 6c). For all tested samples, the drug release profiles started with a burst release, followed by a short period of rapid drug release, ending with an extended slow drug release phase. The high molecular weight associated with the marked hydrophobicity of PCL in the oily core of the NCs can lead to a triphasic release pattern of Doc (29). The drug's initial rapid release is due to a rapid dissolution of drug adsorbed on the surface of the NCs (30). In the second phase, the drug trapping in the polymeric core/shell system could be responsible for the slow release of Doc. The controlled, released phase could be dictated by the polymer erosion and the drug diffusion toward the aqueous release medium. The triphasic drug release behavior from such nanocarriers has been described in a previous work (31). Furthermore, the release mechanism of Doc from the NCs was investigated. For this purpose, data obtained from the *in vitro* release study were fitted to several kinetic equations (21). As shown in Table III, drug release kinetics from F_3, F_6, F_8, F_{12}, F_{13}, and F_{14} were mostly consistent with the first order equation ($r^2 \geq 0.95$), as described in Eq. 4:

$$Log\ Q_t = Log\ Q_0 - K.t/2.303 \quad (4)$$

where Q_0 is the initial amount of drug, Q_t is the cumulative amount of drug at time "t," and K is the first order drug release constant. This indicated that the drug release rate from the oily core NCs depended on its concentration. Interestingly, F_1

Table II Comparison Between Predicted and Experimental Values of Dependent Variables from the Optimal Formula Using Unpaired *T*-Test

PMD (nm ± SD)			EE% (±SD)		
Experimental	Predicted	*p*	Experimental	Predicted	*p*
220.38 ± 10.29	224.18 ± 15.71	0.44	58.42 ± 8.33	60.38 ± 7.70	0.74

and F_8 provided a better fit with the Higuchi model ($r^2 \geq 0.95$) shown in Eq. 5:

$$Q = K_H \sqrt{t} \quad (5)$$

where, Q and K_H are the cumulative amount of drug at time "t" and the Higuchi constant, respectively. This indicated that the release of Doc could also occur by diffusion from the oily core to the release medium. This finding also suggested that the encapsulated Doc was uniformly distributed inside the oily core of NCs (32). However, the drug release kinetics from F_2, F_4, F_5, F_7, F_9, F_{10}, F_{11}, and F_{15} did not fit with any of the selected models ($r^2 < 0.95$, Table III). All the reported data were obtained under sink conditions.

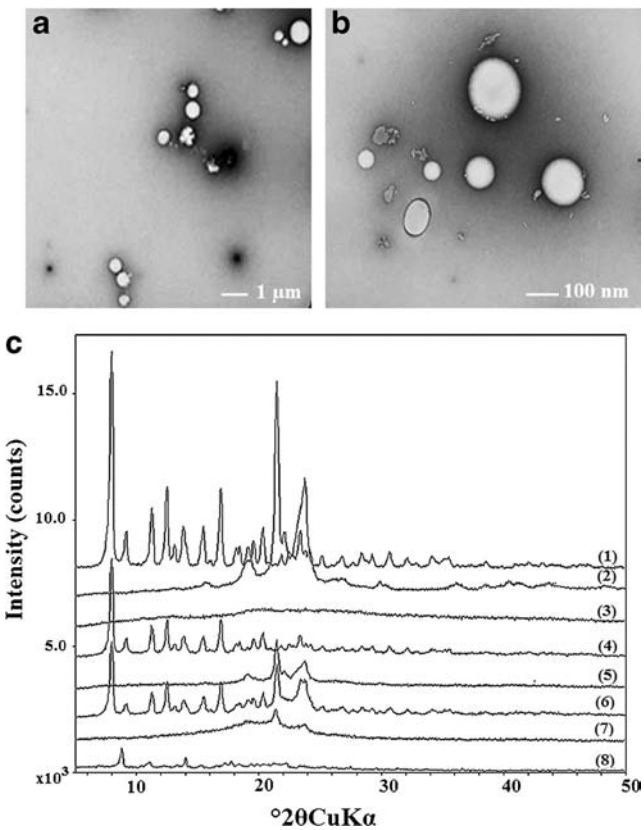

Fig. 5 HA-PEG/PCL-grafted oily core NCs (the optimized formula (F_{opt}) obtained from the experimental design) images obtained by transmission electron microscopy at low (**a**) and high (**b**) magnification, (**c**) Powder X-ray diffraction pattern for (*1*) docetaxel (Doc), (*2*) amine-PEG/PCL, (*3*) Hyaluronic acid (HA, 11 kDa), (*4*) physical mixture of Doc + HA, (*5*) Physical mixture of HA + PCL/PEG, (*6*) Physical mixture of Doc + HA + NH2-PEG/PCL, (*7*) Blank nanocapsules, (*8*) Doc-loaded HA-PEG/PCL-grafted NCs.

Cell Viability Assay

This assay indicated at least 95% of cell viability for samples treated with Blank NCs (control) and a strong correlation between the cytotoxicity and Doc concentrations from the native drug, PEG and HA-PEG/PCL-grafted NCs as well (Fig. 7a). However, higher cytotoxicity of Doc-loaded HA-PEG/PCL-grafted NCs was shown in comparison with that of Doc-loaded PEG NCs and native Doc at high concentrations ($P < 0.05$; 100–10,000 nM). The higher toxicity of HA-PEG/PCL-grafted NCs might be attributed to the presence of HA

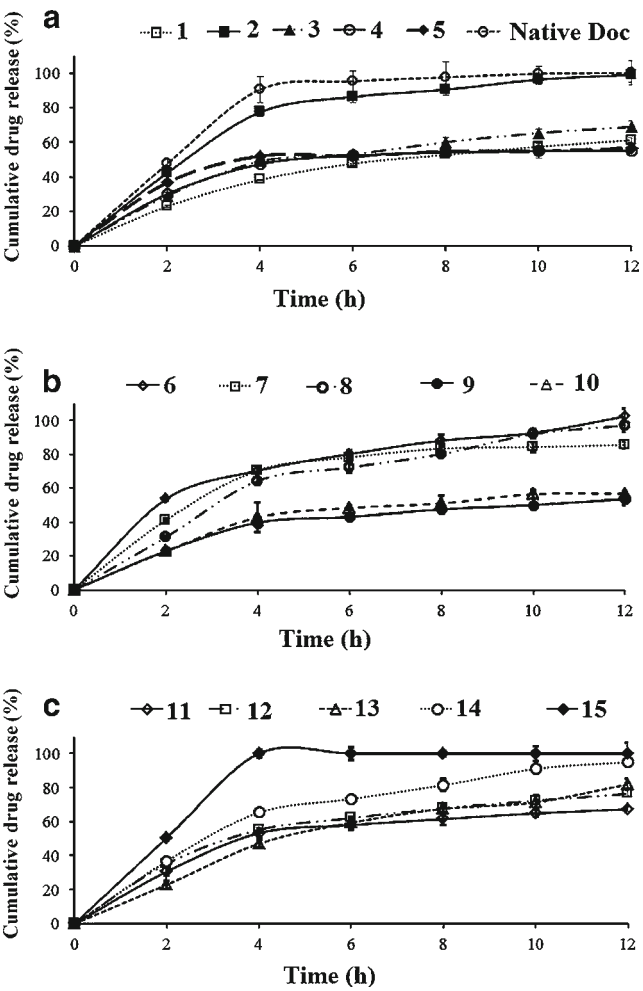

Fig. 6 Cumulative drug release from *selected* docetaxel-loaded hyaluronic acid-PEG/PCL-grafted nanocapsules: (**a**) F_1, F_2, F_3, F_4 and F_5; (**b**) F_6, F_7, F_8 F_6, F_9 F_{10}; (**c**) F_{11}, F_{12}, F_{13}, F_{14}, F_{15},. The composition and the physicochemical characteristics of these formulations are shown in Table II.

Table III Values of the coefficient of determination (r^2), *K* and *n* Values Obtained from Drug Release Data of Various Nanoformulations of Docetaxel-Loaded Hyaluronic Acid-Polyethylene Glycol/ Polycaprolactone-Grafted Oily Core Nanocapsules

Formulation	Zero order		First order		Higuchi		Korsmeyer-Peppas	
	$K_0(h^{-1})$	r^2	$-k/2.303$	r^2	K_H ($h^{-1/2}$)	r^2	n	r^2
F_1	3.55	0.90	0.03	0.94	18.26	0.96	0.54	0.96
F_2	4.98	0.79	0.22	0.85	31.71	0.82	0.45	0.89
F_3	3.65	0.90	0.03	0.96	21.05	0.93	0.46	0.95
F_4	2.14	0.68	0.02	0.73	18.64	0.43	0.33	0.85
F_5	1.47	0.60	0.01	0.63	19.14	0.85	0.21	0.79
F_6	4.57	0.96	0.10	0.99	21.20	0.85	0.35	0.99
F_7	3.84	0.72	0.06	0.86	28.35	0.68	0.39	0.86
F_8	6.00	0.90	0.13	0.95	28.65	0.95	0.60	0.93
F_9	2.69	0.85	0.02	0.90	16.58	0.88	0.45	0.92
F_{10}	3.02	0.81	0.02	0.87	17.98	0.88	0.49	0.90
F_{11}	3.17	0.79	0.03	0.87	21.53	0.78	0.42	0.89
F_{12}	3.76	0.89	0.04	0.96	23.74	0.89	0.42	0.96
F_{13}	5.38	0.92	0.06	0.98	23.16	0.95	0.68	0.96
F_{14}	5.37	0.89	0.11	0.98	23.79	0.95	0.51	0.95
F_{15}	3.54	0.43	0.10	0.43	64.81	0.18	0.34	0.66
F_{16}	5.01	0.84	0.17	0.88	22.13	0.97	0.51	0.97
F_{17}	5.36	0.77	0.14	0.96	33.14	0.95	0.46	0.95
F_{18}	5.23	0.81	0.12	0.97	29.08	0.95	0.48	0.95

on the surface of the NCs. Indeed, HA targeting nanocarrriers have been demonstrated to increase drug accumulation on CD44 *bearing* cells (33). Therefore, HA could be a potential target for CD44-positive cancer cells.

Determination of the Intracellular Concentration of Reactive Oxygen Species

At low concentrations of Doc (<100 nM), the concentrations of ROS between samples treated with native Doc, Doc-loaded PEG and HA-PEG/PCL-grafted NCs were comparable ($P>0.05$, Fig. 7b). However, at high concentration of Doc, the intracellular concentration of ROS from samples treated with HA-PEG/PCL-grafted NCs were lower than that of native Doc and Doc-loaded-PEG NCs treated cells ($P<0.05$). This indicated that a certain concentration of HA was required to significantly decrease the production of intracellular ROS. This latter finding was in accordance with a previous work, demonstrating the ROS-scavenging property of HA leading to a decrease of the intracellular concentration of ROS (34).

Determination of the Intracellular Concentration of Reduced Glutathione

The intracellular concentration of the reduced glutathione (GSH) was investigated by microplate reader in MDA-MB 231 cells. From Fig. 7c, no significant difference between treated samples was detected at low concentrations of Doc (0.1–10 nM). However, at high concentration of Doc (100–10,000 nM), samples treated with HA-PEG/PCL-grafted NCs significantly exhibited higher increases of intracellular concentrations of GSH compared to that of Doc-loaded PEG NCs. This indicated that HA could induce a protective effect against this oxidative agent through the generation of intracellular GSH. In this concentration range, the increase of the intracellular level of GSH did not interfere with the cytotoxicity of Doc released from HA-PEG/PCL-grafted NCs. This finding correlated well with the above results showing the reduced effect of HA on the ROS generation. This finding revealed a paradoxal effect of HA in eliminating malignant cells while contributing in the detoxification of oxidative agents, such as ROS, that could synergically enhance the toxicity against malignant cells. The high expression level of CD44 was also reported to enhance the intracellular level of GSH (35). Bearing in mind that MDA-MB 231 is a CD44-overexpresssing cell line (36), the effect of HA on the intracellular level of GSH could be cell-dependent. Overall cytotoxicity results, including mitochondria damage, ROS, and GSH, contributed to elucidate the mode of action of the toxicity of Doc-loaded HA-PEG/PCL NCs in MDA-MB 231 cells.

Particle Cellular Uptake Study by Flow Cytometry Analysis

The results indicated that the particle cellular uptake was concentration-dependent for both HA-grafted and ungrafted

NCs (Fig. 8a and b). The particle cellular internalization result consistently showed a significant enhancement of HA-PEG/PCL-grafted NCs uptake (up to 4 fold) in comparison with PEG NCs. This finding could also be correlated with the high toxicity of Doc-loaded HA-PEG/PCL-grafted NCs shown from MTS results. A possible explanation is that the presence of HA on the surface of the NCs contribute to enhance the particle cellular uptake efficacy through the high binding affinity of HA to the extracellular domain of the CD44 receptor in the MDA-MB 231 cells. Previous work has demonstrated that pegylated HA nanoparticles were uptaken more than non-pegylated HA-nanoparticles (1.6 fold) in tumor tissue (37). Here, we demonstrated that HA-PEG/PCL-grafted NCs exhibited a higher uptake compared to PEG NCs.

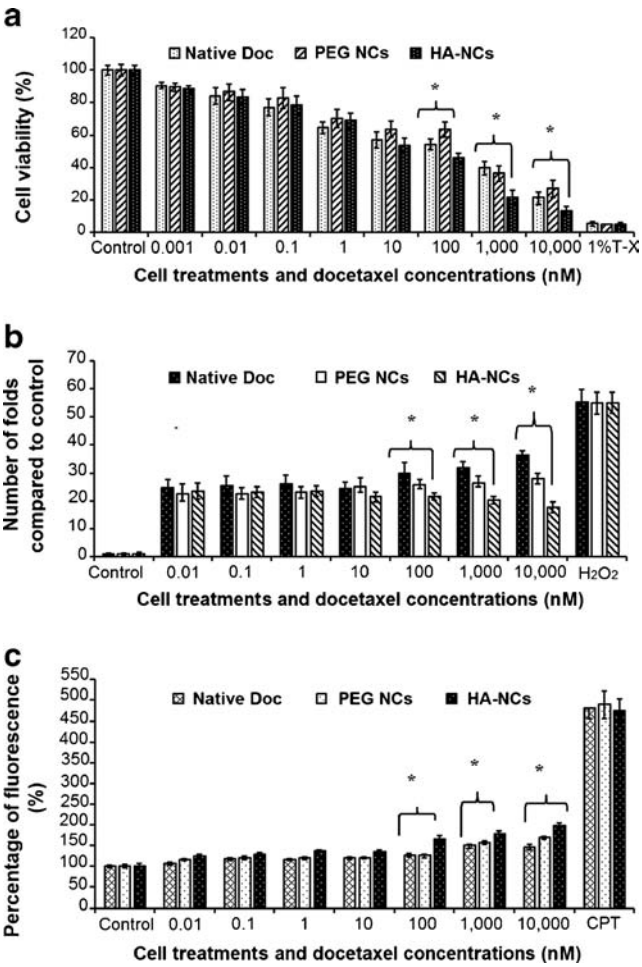

Fig. 7 *In vitro* evaluation of the cytotoxicity of docetaxel-loaded HA-PEG/PCL and blank nanocapsules (NCs) in MDA-MB 231 cells after 24 h exposure by (**a**) MTS assays using 1%Triton-X 100 as positive control (**b**) Reactive oxygen species (ROS) generation using hydrogen peroxide (H_2O_2) as positive control; (**c**) Reduced glutathione (GSH) intracellular concentration using camptothecin (CPT) as positive control. Three groups of cells were treated with Docetaxel, Pegylated NCs and HA-Pegylated NCs. Data are normalized (control = 100%) and expressed as the mean percent ± Standard deviation (SD) from six measurements ($n = 6$). *Stars* indicate significant difference from the respective control with $*p \leq 0.05$, $**p \leq 0.01$.

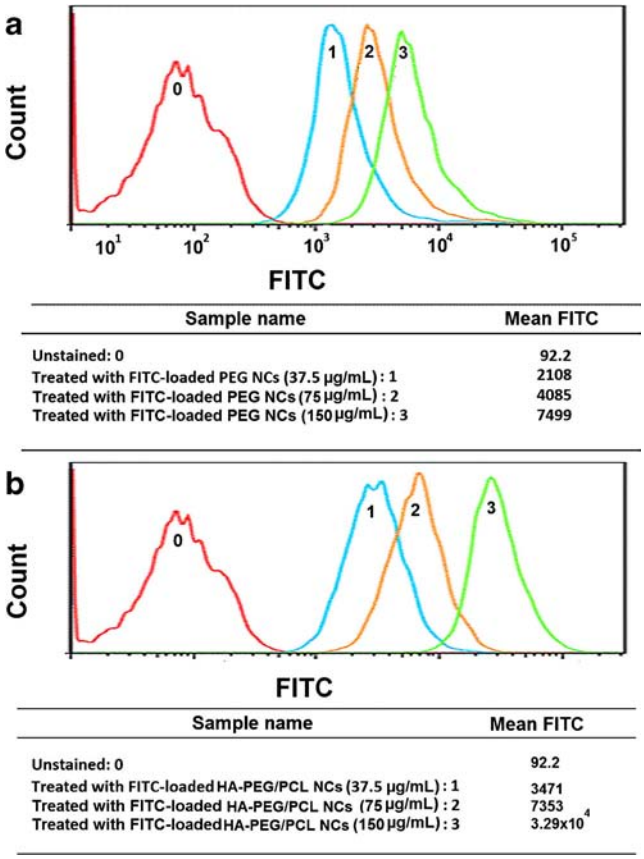

Fig. 8 Cellular uptake of fluorescein isothiocyanate (FITC)-loaded NCs evaluated by flow cytometry in MDA-MB 231 cells: Count vs FITC-fluorescence intensity (**a**) PEG-NCs related data: Unstained (0), cells treated with FITC-loaded PEG-NCs [37.5 μg/mL, (1); 75 μg/mL (2) and 150 μg/mL (3)] and (**b**) HA-PEG/PCL-NCs related data: Unstained (0), cells treated with FITC-loaded HA-PEG/PCL NCs [37.5 μg/mL, (1); 75 μg/mL (2) and 150 μg/mL (3)].

Particle Cellular Uptake Study by Confocal Microscopy

The FITC channel was used to observe the NCs and that of PI was used to observe the cell nucleus. The results indicated that both PEG and HA-PEG/PCL-grafted NCs were taken up by MDA-MB 231 cells (Fig. 9a and b). In addition, a cross comparison between PEG NCs (Fig. 9a) and HA-PEG/PCL grafted NCs (Fig. 9b) indicated higher cellular uptake of HA-PEG/PCL-grafted NCs. In order to demonstrate the involvement of the CD44 receptor in the uptake efficacy of HA-PEG/PCL NCs, an anti CD44 antibody was employed to competitively inhibit the HA binding to the CD44 receptor *as further discussed below*.

Elucidating the Involvement of CD44 Receptor in Nanocapsule Cellular Uptake

In vitro particle cellular uptake indicated an enhanced intracellular uptake (~3 to 4-fold) in MDA-MB 231 cells compared to NIH3T3 cells (Fig. 9c). *Furthermore,* a pairwise comparison

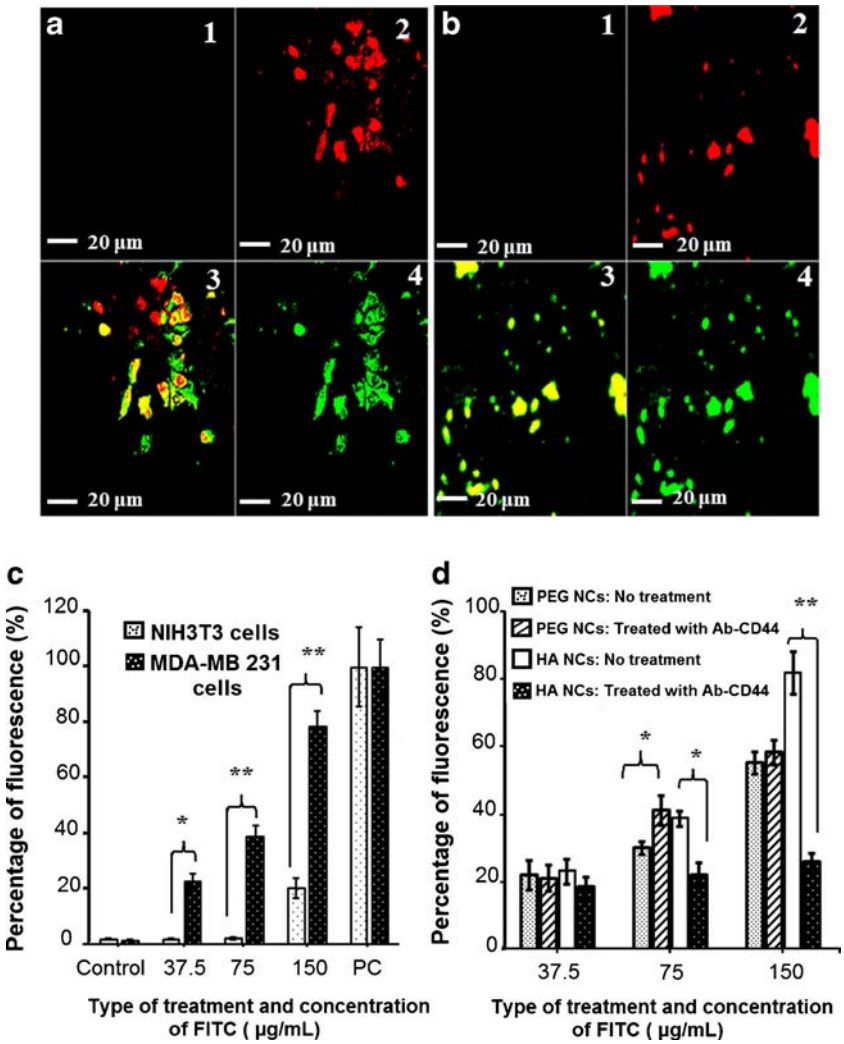

Fig. 9 (**a**-**b**) Confocal microscopy images after 24 h exposure with 150 μg/mL of each of the two types of FITC-loaded NCs: Background (1); Stained cell nuclei with propidium iodide (2); FITC-loaded NCs (3) and merged images (4). (**a**): Images related to PEG-NCs. (**b**): images related to HA-PEG/PCL NCs. (**c**) *In vitro* particle cellular uptake in NIH 3 T3 (CD44-negative) and MDA-MB 231 (CD44-positive) cell lines. (**d**) Particle cellular uptake inhibition (in MDA-MB 231 cells)-mediated HA/CD44 after treatment with antibody anti-CD44 and incubation with FITC-loaded PEG NCs *versus* HA-PEG-PCL NCs at three different concentrations (37.5, 75 and 150 g/mL. *Stars* indicate significant difference from the respective control with $*p \leq 0.05$, $**p \leq 0.01$.

between treated and untreated samples was conducted to demonstrate the involvement of the CD44 receptor in the internalization of HA-PEG/PCL-grafted NCs. As shown, no significant difference was observed at low concentration of FITC (37.5 µg/mL) for both types of NCs (Fig. 9d). At medium and high concentrations of FITC (75 and 150 µg/mL), the internalization of the PEG NCs seemed not to be affected by the cells pretreatment with an anti CD44 antibody. However, the uptake of HA-PEG/PCL-grafted NCs was markely decreased after pretreatment with an anti CD44 antibody at medium and high concentration of FITC compared to that of PEG NCs. In this concentration range, the internalization of the HA-PEG/PCL appeared to be mediated by the CD44 receptor. Indeed, the CD44 antibody can bind to the extracellular domain of the CD44 receptor located in a repeated sequences of positively charged amino acids avoiding the availability of HA binding sites (38). The current finding clearly showed the evidence of the CD44 mediated uptake pathway of the HA-PEG/PCL-grafted NCs, thus supporting the above hypothesis. This finding also suggested that a certain level of FITC-loaded HA-PEG/PCL-grafted NCs is required for an efficient particle uptake *via* CD44, as described in a previous work using HA-grafted liposomes (39). So far, the mechanism of the HA binding to the CD44 is still not understood.

CONCLUSIONS

HA-PEG/PCL-grafted NCs has been successfully synthesized *for the first time* by surfactant-free emulsion-solvent diffusion method, optimized using BBD and tested on *both CD44 positive and negative cell lines*. The optimal Doc-loaded HA oily core NCs had respective PMD, polydispersity, and drug encapsulation efficiency of 224±15.71 nm, 0.32±0.11, and 60.38±7.70%. After formulation, the native crystalline drug became partially amorphous. *In vitro*, the synthesized blank NCs exhibited at least 95% of cell viability. Doc-loaded HA-PEG/PCL-grafted NCs could enhance the cellular uptake and anticancer activity when compared to PEG NCs in MDA-MB 231 cells. The generation of ROS

was attenuated in the presence of HA. Moreover, the production of GSH was enhanced by Doc-loaded HA-PEG/PCL-grafted NCs. Interestingly, the internalization of HA-PEG/PCL-grafted NCs was shown to be mediated by the CD44 receptor in MDA-MB 231 cells. The present study demonstrates that Doc-loaded HA-PEG/PCL-grafted oily core NCs can enhance the drug cytotoxicity and uptake in CD44 expressing BC cells. The major outcome of this present work sustains that HA-PEG/PCL-grafted NCs could be an emerging platform for breast cancer diagnosis and therapy. Future work will visualize and characterize the in vivo biodistribution, safety and efficacy of HA-PEG/PCL-grafted NCs in mice bearing tumor.

ACKNOWLEDGMENTS AND DISCLOSURES

The work was supported by UMKC School of Pharmacy Dean internal bridge/seed funds. The authors acknowledge Gattefossé Corporation (Saint-Priest, France) for providing a gift sample of Labrafac CC oil. We gratefully acknowledge Mr. Jack Liu (Zhenjiang Dong Yuan Biotech Co., Ltd., Jiangsu, China) for providing samples of hyaluronic acid. We also thank Richard Hastings at Kansas University for his assistance with the flow cytometry analysis. We are grateful to Dr. Jeffrey L. Price for providing assistance with the confocal laser scanning microscopy at the University of Missouri, Kansas City; School of Biological Sciences. The authors appreciate the helpful discussions on ROS and GSH assay with Dr. Miezan JM Ezoulin (Post-doctoral research associate at the University of Missouri Kansas City; School of Pharmacy. The assistance of Jianing Meng (Graduate student at the University of Missouri Kansas City School of Pharmacy) for the figure graphic design is appreciated. The authors thank Barbara Fegley for her assistance with the Electron microscopy at University of Kansas Medical Center, Kansas City, Kansas.

REFERENCES

1. Berezhnoy A, Brenneman R, Bajgelman M, Seales D, Gilboa E. Thermal stability of siRNA modulates aptamer- conjugated siRNA inhibition. Mol Ther Nucleic Acids. 2012;1:e51.
2. Oh Y-K, Park TG. siRNA delivery systems for cancer treatment. Adv Drug Deliv Rev. 2009;61(10):850–62.
3. Arap W, Pasqualini R, Ruoslahti E. Cancer treatment by targeted drug delivery to tumor vasculature in a mouse model. Science. 1998;279(5349):377–80.
4. Zhang K, Sefah K, Tang L, Zhao Z, Zhu G, Ye M, *et al.* A novel aptamer developed for breast cancer cell internalization. Chem Med Chem. 2012;7(1):79–84.
5. Jin YJ, Termsarasab U, Ko SH, Shim J-S, Chong S, Chung S-J, *et al.* Hyaluronic acid derivative-based self-assembled nanoparticles for the treatment of melanoma. Pharm Res. 2012;29(12):3443–54.
6. Tsai SW, Fang JF, Yang CL, Chen JH, Su LT, Jan SH. Preparation and evaluation of a hyaluronate-collagen film for preventing post-surgical adhesion. J Int Med Res. 2005;33(1):68–76.
7. Lopez JI, Camenisch TD, Stevens MV, Sands BJ, McDonald J, Schroeder JA. CD44 attenuates metastatic invasion during breast cancer progression. Cancer Res. 2005;65(15):6755–63.
8. Naor D, Sionov RV, Ish-Shalom D. CD44: structure, function, and association with the malignant process. Adv Cancer Res. 1997;71:241–319.
9. Ahrens T, Sleeman JP, Schempp CM, Howells N, Hofmann M, Ponta H, *et al.* Soluble CD44 inhibits melanoma tumor growth by blocking cell surface CD44 binding to hyaluronic acid. Oncogene. 2001;20(26):3399–408.
10. de la Torre M, Heldin P, Bergh J. Expression of the CD44 glycoprotein (lymphocyte-homing receptor) in untreated human breast cancer and its relationship to prognostic markers. Anticancer Res. 1995;15(6B):2791–5.
11. Bourguignon LYW, Singleton PA, Zhu H, Zhou B. Hyaluronan promotes signaling interaction between CD44 and the transforming growth factor β receptor I in metastatic breast tumor cells. J Biol Chem. 2002;277(42):39703–12.
12. Ma Y, Zeng Y, Zeng X, Jiang L, Cheng H, Liu R, *et al.* Novel docetaxel-loaded nanoparticles based on PCL-Tween 80 copolymer for cancer treatment. Int J Nanomedicine. 2011;6:2679–88.
13. Ren S-T, Liao Y-R, Kang X-N, Li Y-P, Zhang H, Ai H, *et al.* The antitumor effect of a new docetaxel-loaded microbubble combined with low-frequency ultrasound in vitro: preparation and parameter analysis. Pharm Res. 2013;30(6):1574–85.
14. Huynh N, Morille M, Bejaud J, Legras P, Vessieres A, Jaouen G, *et al.* Treatment of 9 L gliosarcoma in rats by ferrociphenol-loaded lipid nanocapsules based on a passive targeting strategy via the EPR effect. Pharm Res. 2011;28(12):3189–98.
15. Box GEP, Behnken DW. Some new three level designs for the study of quantitative variables. Technometrics. 1960;2(4):455–75.
16. Chan JM, Valencia PM, Zhang L, Langer R, Farokhzad OC. Polymeric nanoparticles for drug delivery. Methods Mol Biol. 2010;624:163–75.
17. Quintanar-Guerrero D, Allémann E, Doelker E, Fessi H. Preparation and characterization of nanocapsules from preformed polymers by a new process based on emulsification-diffusion technique. Pharm Res. 1998;15(7):1056–62.
18. Youm I, Murowchick JB, Youan BBC. Entrapment and release kinetics of furosemide from pegylated nanocarriers. Colloids Surf B: Biointerfaces. 2012;94(1):133–42.
19. Hackley V, Ferraris C. The use of nomenclature in dispersion science and technology. SP: NIST Recommended Practice Guide; 2001.
20. Venishetty VK, Parikh N, Sistla R, Ahmed FJ, Diwan PV. Application of validated RP-HPLC method for simultaneous determination of docetaxel and ketoconazole in solid lipid nanoparticles. J Chromatogr Sci. 2011;49(2):136–41.
21. Costa P, Sousa Lobo JM. Modeling and comparison of dissolution profiles. Eur J Pharm Sci. 2001;13(2):123–33.
22. Haugland R. Handbook of fluorescent probes and research chemicals. 6 ed. Eugene: Molecular Probes; 1996.
23. Kaur P, Aschner M, Syversen T. Glutathione modulation influences methyl mercury induced neurotoxicity in primary cell cultures of neurons and astrocytes. Neurotoxicology. 2006;27(4):492–500.
24. Yetilmezsoy K, Demirel S, Vanderbei RJ. Response surface modeling of Pb(II) removal from aqueous solution by pistacia vera L.: box-behnken experimental design. J Hazard Mater. 2009;171(1–3):551–62.
25. Liu Y, Sun J, Cao W, Yang J, Lian H, Li X, *et al.* Dual targeting folate-conjugated hyaluronic acid polymeric micelles for paclitaxel delivery. Int J Pharm. 2011;421(1):160–9.
26. Zaske L, Perrin MA, Leveiller F. Docetaxel: solid state characterization by X-ray powder diffraction and thermogravimetry. J Phys IVFrance 11. 2001.
27. Youm I, Yang X, Murowchick J, Youan BBC. Encapsulation of docetaxel in oily core polyester nanocapsules intended for breast cancer therapy. Nanoscale Res Lett. 2011;6(1):630.

28. Abdelwahed W, Degobert G, Fessi H. A pilot study of freeze drying of poly(epsilon-caprolactone) nanocapsules stabilized by poly(vinyl alcohol): formulation and process optimization. Int J Pharm. 2006;309(1–2):178–88.
29. Na DH, DeLuca PP. PEGylation of octreotide: I. Separation of positional isomers and stability against acylation by Poly(D, L-lactide-co-glycolide). Pharm Res. 2005;22(5):736–42.
30. Huang X, Brazel CS. On the importance and mechanisms of burst release in matrix-controlled drug delivery systems. J Control Release. 2001;73(2–3):121–36.
31. Luo Y, Ling Y, Guo W, Pang J, Liu W, Fang Y, *et al.* Docetaxel loaded oleic acid-coated hydroxyapatite nanoparticles enhance the docetaxel-induced apoptosis through activation of caspase-2 in androgen independent prostate cancer cells. J Control Release. 2010;147(2):278–88.
32. Lai MK, Chang CY, Lien YW, Tsiang RC. Application of gold nanoparticles to microencapsulation of thioridazine. J Control Release. 2006;111(3):352–61.
33. Platt VM, Szoka FC. Anticancer therapeutics: targeting macromolecules and nanocarriers to hyaluronan or CD44, a hyaluronan Receptor. Mol Pharm. 2008;5(4):474–86.
34. Karihtala P, Soini Y, Auvinen P, Tammi R, Tammi M, Kosma V-M. Hyaluronan in breast cancer: correlations with nitric oxide synthases and tyrosine nitrosylation. J Histochem Cytochem. 2007;55(12):1191–8.
35. Ishimoto T, Nagano O, Yae T, Tamada M, Motohara T, Oshima H, *et al.* CD44 variant regulates redox status in cancer cells by stabilizing the xCT subunit of system xc(-) and thereby promotes tumor growth. Cancer Cell. 2011;19(3):387–400.
36. Sheridan C, Kishimoto H, Fuchs R, Mehrotra S, Bhat-Nakshatri P, Turner C, *et al.* CD44+/CD24- breast cancer cells exhibit enhanced invasive properties: an early step necessary for metastasis. Breast Cancer Res. 2006;8(5):R59.
37. Choi KY, Min KH, Yoon HY, Kim K, Park JH, Kwon IC, *et al.* PEGylation of hyaluronic acid nanoparticles improves tumor targetability in vivo. Biomaterials. 2011;32(7):1880–9.
38. Peach RJ, Hollenbaugh D, Stamenkovic I, Aruffo A. Identification of hyaluronic acid binding sites in the extracellular domain of CD44. J Cell Biol. 1993;122(1):257–64.
39. Qhattal S, Liu X. Characterization of CD44-mediated cancer cell uptake and intracellular distribution of hyaluronan-grafted liposomes. Mol Pharm. 2011;8(4):1233–46.